# Behavior of the rate constant for reactions in restricted spaces: Fluorescence probing of lipid vesicles

P. Argyrakis
*Department of Physics 313-1, University of Thessaloniki, 54006 Thessaloniki, Greece*

G. Duportail
*Centre de Recherches Pharmaceutiques, Laboratoire de Physique, UA CNRS 491, Universite Louis Pasteur, B. P. 24, 67401 Ilkirch Cedex, France*

P. Lianos
*University of Patras, School of Engineering, 26000 Patras, Greece*

The bimolecular reaction A + B→products, where [A] < [B], was studied by fluorescence probing of small unilamellar vesicles of dipalmitoylphosphatidylglycerol with pyrene, and by computer simulation on a square lattice containing nonpercolating clusters. The decay curves of the minority species were fitted with an equation obtained from the theory of random walks in fractal domains. The analysis of the data has allowed redefinition of the reaction rate in restricted geometries, which is now time dependent, and sets the basis for simple treatment of bimolecular reactions in organized assemblies. The values of the spectral dimension calculated from this work are in the range 0.35–0.66, where the upper limit reflects the Alexander–Orbach conjecture, and the lower values are used to monitor the solubilizate aggregation in vesicles.

## I. INTRODUCTION

The study of reactions in microheterogeneous phases is a subject of prime importance from both physicochemical and biophysical point of view, since reaction rates in such phases are largely influenced by the particular environment they provide. One of the main characteristics of this environment is the low dimensionality which makes reactions proceed in a very different and restricted manner from homogeneous solutions. The recent advances of fractal geometry have accelerated our understanding of the dimensionality effect on the reaction rates, and have also helped to unify the applied models by introducing the concept of noninteger dimension.

Most of the works published so far deal with the study of direct energy transfer (DET), or energy migration in solids. The theoretical models developed also refer mainly to such processes. DET depends on the spatial distribution of the acceptors with respect to donor molecule,[1-4] thus it involves the geometry of the reaction domain. If the domain is self-similar (i.e., it is fractal), then DET depends primarily on the fractal dimension $d_f$ of the reaction domain.[1-4] However, when energy migrates, the dimensionality sensed depends not only on the geometry but also on the path followed (by the random walker) which might involve repeated visits to available sites. It has been found that the dimensionality of migration is expressed by the spectral dimension $d_s$ which is given[5] by $d_s = 2d_f/d_w$, where $d_w$ is the fractal dimension of the path. Alternatively, the number of distinct sites visited by the migrating random walker is expressed[6-11] as $S(t) \sim t^{d_s/2}$, where time $t$ is proportional to the number of random walk steps. This expression is rather an approximation, theoretically obtained at $t = \infty$, but, it has been shown that the asymptotic domain is reached very rapidly.[12]

When a donor is excited by a short pulse, its decay is an exponential function with a complicated argument containing an infinite number of terms.[13] To treat the experimental results, several approximations have been made by reasoning mainly in terms of dimensionality itself. The lowest-order approximation appears in the form of a stretched exponential, i.e., $\ln[F(t)] \sim t^x$, where $0 < x < 1$ and $F(t)$ is the survival probability. Such a decay is always expected at relatively long times.[11]

This is in very general terms the experience obtained with energy transfer in solid matrices. On the other hand, liquid-state microheterogeneous systems have mainly been studied with diffusion-controlled quenching processes in numerous fluorescence probing studies. It is of interest to test the concept of dimensionality in molecular diffusion and interactions, in order to study, under new light, the structure and dynamics of such microheterogeneous systems as lipid vesicles,[14-16] as well as micelles and microemulsions.[17-20]

In diffusion-controlled processes of the A + B type where the reaction is monitored by luminescence (i.e., diffusion-controlled quenching) both types of reactants can diffuse during the lifetime of the excited state. We have thus modeled the *mutual* diffusion as a random walk of a reacting molecule with respect to the other. Each random step is made from one solubilization site to another and multiple visits are possible. In principle, the number of solubilization sites is much larger than the number of quenchers, i.e., the occupation probability $c \ll 1$, but $c$ is not negligible in restricted geometries, i.e., the number of sites is limited. Thus, the diffusion is monitored by the spectral dimension, such that $d_s < 2$. The number of distinct sites visited $S(t)$ will then be asymptotically proportional to $t^{d_s/2}$, as discussed above. Subsequently, the reaction rate, which is given by the time derivative[8] of $S(t)$, will be

$$k(t) \sim \frac{d_s}{2t^{1-d_s/2}} = \frac{f}{t^{1-f}}, \tag{1}$$

where $f = d_s/2$. Naturally, the reaction rate is time dependent, unlike the classical reactions, but as expected for restricted reactions. The decay then of an excited lumophore in the presence of quenchers, at long times, following pulse excitation, will be given by

$$I(t) = I_0 \exp(-k_0 t)\exp(-C_1 t^f), \qquad (2)$$

where $C_1 = k'Q$, $k_0$ is the luminescence decay rate in the absence of quenching, $k'$ is a constant, and $Q$ is the quencher concentration. In a nonrestricted reaction where $f = 1$, Eq. (2) takes the "classical" form where $k'$ is the second-order rate constant. When $f < 1$, the reaction rate is time dependent and it will, obviously, be given by

$$k(t) = \frac{fk'}{t^{1-f}}. \qquad (3)$$

However, in an exact treatment of diffusion where both short and long times are taken into consideration, the exponential argument is an infinite series.[13] Since the random walk of a lumophore towards a quencher is a similar process as the random walk of the migrating excitation, we have approximated the infinite series by an expression employed in energy migration and involving the spectral dimension.[7,15] For an excitation by a short pulse, the decaying fluorescence intensity is given by[15]

$$I(t) = I_0 \exp(-k_0 t)\exp(-C_1 t^f + C_2 t^{2f}), \qquad (4)$$

where $C_1 = k'Q$ and $C_2$ is a constant dependent on $Q$.[7,13,15] In this improved approximation the term $C_1 t^f$ is associated with the average $S(t)$, as above, and the term $C_2 t^{2f}$ with the corresponding variance.[7] It is obvious that Eq. (2) is the lowest-order approximation, and Eq. (4) one order higher approximation of the same general expression. Simulations previously reported have shown that the order of the approximation decreases as the dimensionality increases.[10,11,21] It must be underlined at this point that in the so-called "target problem,"[11] where the excited molecule is considered an immobile target for possible mobile quenchers, the long-time behavior of the decay does not foresee the existence of the term $C_2 t^{2f}$ in Eq. (4), i.e., it is satisfied by first-order approximation. Of course, diffusion-controlled quenching is neither a migration towards a trap nor a target problem. Equation (4) was adopted on experimental grounds. In the present work we apply the above principles to study the bimolecular reaction $A + B \rightarrow$ products, where $[A] < [B]$, in the restrictive environment provided by nonpercolating clusters. The work contains two parts: simulations on a square lattice, and experimental study of the fluorescence of pyrene in small unilamellar vesicles. The employment of models devised for solid matrices with liquids is justified in the sense that vesicles are considered invariable in the time domain of a few hundred nanoseconds, which is the scale of the present fluorescence measurements. The simulation results are compared with the experimental results directly. Emphasis is given on the variation of reactant concentration. The analysis of the ensemble helps us to redefine the reaction

rate in restricted geometries, and thus permits a simple treatment for reactions in lipid vesicles.

## II. COMPUTATIONAL METHODS

The computer simulation of the fluorescence-quenched reaction was done using techniques previously reported.[22] Briefly, lattice clusters are generated on a $300 \times 300$ square lattice at a given probability $p$ of an open site, which in this work was fixed at $p = 0.50$. A minimum and a maximum cluster size $s$ are also specified in order to represent actual experimental situations in a more realistic manner. For this reason only the clusters that fall into this prescribed range are kept, while all the rest become nonaccessible sites. A certain number of A and B particles are placed at random on the available clusters at time $t = 0$. Reaction proceeds in the known way, i.e., all particles perform random walks with the stipulation that when A and B particles occupy the same site they annihilate and are removed from the system, while nothing happens between two A or two B particles. We use exclusion volume principles, i.e., we do not allow more than one particle to occupy simultaneously the same site. We monitor the concentration [A] of A particles (i.e., the minority species representing the excited fluorophore) as a function of time. The basis for our time unit is one Monte Carlo step (MCS), which is defined as the time it takes for a particle to move to its nearest neighbor. In the present calculation time changes from 0 to 200. If we assume that 1 MCS is equivalent to the time order of a few nanoseconds, then the real situation of pyrene monomer decay is nicely represented by the present simulation. We have monitored several interactions by varying both $s$ and the ratio $[B]_0/[A]_0$, where the subscript 0 denotes initial concentrations. Thus the lower limit for $s$ was fixed at 25 sites and the higher limit was 50, 250, and $\infty$ (here $\infty$ means the total finite lattice). The ratio $[B]_0/[A]_0$ was varied between 1.0 and 20.0. We have in fact performed two series of simulations, named case I and case II. In case I, $[A]_0$ was constant, equal to 100 particles/volume, and $[B]_0$ was continuously increased. In case II, $[B]_0$ was constant, equal to 2000 particles/volume, and $[A]_0$ was continuously decreased. It should be underlined that by assuming a uniform time distribution and by making all available sites equivalent, no time dispersion and no energetic dispersion has been taken into account.[10,23] Thus the analysis focuses at only purely dimensionality (geometrical) considerations. The representation of the interaction between an excited fluorophore and a quencher, both solubilized in a medium embedded in a three-dimensional (3D) space, by the species A and B placed on a two-dimensional (2D) lattice, does not limit generality. In any case, the vesicle bilayer has a limited dimensionality. Nevertheless, simulations in 3D lattices give similar trends as in 2D lattices, even though the obtained data might differ in absolute values. For example, the percolation threshold is $p_c = 0.59$ for 2D, but only $p_c = 0.31$ for 3D lattices. However, the spectral dimension $d_s = 1.33$ is valid for both lattices. Thus, the choice of 2D is made only to economize in computer time. Finally, the choice of $p = 0.50$ in the present case refers to a situation below critical percolation (all clusters separated), in an ef-

fort to represent vesicles which are considered nonpercolating structures.

## III. EXPERIMENTAL METHODS

Small unilamellar vesicles (SUV) of dipalmitoylphosphatidylglycerol (DPPG, from Sigma), labeled with pyrene, were prepared as previously described.[15] Each sample was characterized by its phospholipid and pyrene concentrations (see Sec. IV). The concentrations of pyrene embedded in vesicles were checked by both absorption and fluorescence spectroscopy. The fluorescence decay profiles were recorded with a time-correlated photon-counting apparatus equipped with a hydrogen flash lamp. An interference filter at 385 nm (Schott, Mainz) was used to monitor the pyrene monomer emission. To avoid quenching of fluorescence by oxygen, all samples were deoxygenated by bubbling with $N_2$ for 30 min. The decay time of free pyrene monomer (without excimer) was measured by utilizing samples containing pyrene at concentration $[P] < 10^{-6}$ M. The fluorescence decay profiles were analyzed with least-square fits. The criteria for the quality of the fit were the distribution and the autocorrelation function of the residuals, and the value of chi-square, which was always close to 1.00. The time profile of the excitation pulse (see Fig. 1) was judged wide enough to necessitate convolution of the applied model. Indeed, Eq. (4) was used in the following form:

$$F_i = A \left( \sum_{j=1}^{i} G_j \exp[ -k_0 w(i-j) \right.$$
$$\left. \times \exp\{ -C_1 [w(i-j)]^f + C_2 [w(i-j)]^{2f}\} \right),$$

(5)

where $F_i$ corresponds to the experimental value of the fluorescence intensity at channel $i$, $A$ is a fitted parameter, $G_j$ is the value of the intensity of the exciting pulse at channel $j$, and $w$ is the time interval between two channels (presently 1.87 ns). The fitting started 38 channels after the point where the exciting pulse starts rising, in order to avoid interference from scattered light, which is always present in solutions containing lipid vesicles.

## IV. RESULTS

### A. Computer simulations

The data obtained by monitoring the concentration of [A] vs the number of MCS (i.e., time) were fitted with Eq. (4). Of course, since [A] is not measured by fluorescence, Eq. (4) was used without the factor $\exp( -k_0 t)$. The fit was very good, as in previous similar cases (see, for example, Fig. 1 of Ref. 22). The constant $C_2$ was found in all cases different from zero, as expected in highly restricted environments of low dimensionality. The values of $f$ and $C_1$ obtained dur-
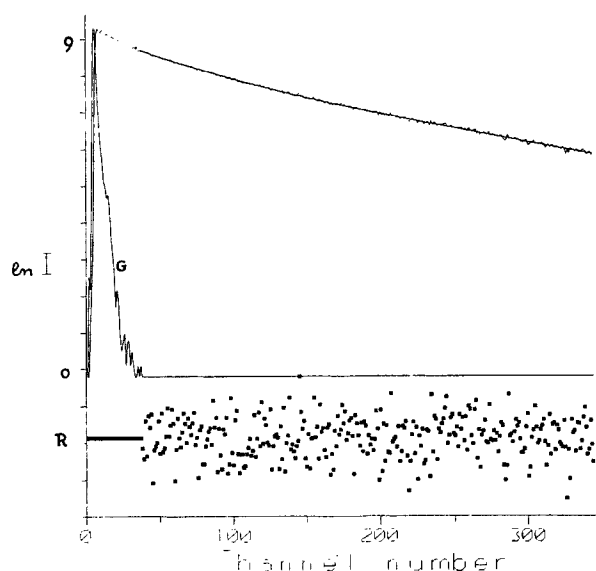


FIG. 1. Monomer fluorescence decay profile of $2 \times 10^{-5}$ M pyrene in $3.5 \times 10^{-4}$ M DPPG together with fitted curve, the exciting pulse (G), and the distribution of the residuals (R). The value of $X^2$ for this fit was 1.03.

ing the fitting procedure are shown in Tables I and II for various sizes $s$ and various $[B]_0/[A]_0$ ratios. Table I shows the results of case I ($[A]$ constant) and Table II those of case II ($[B]$ constant). Both $f$ and $C_1$ were used to calculate the corresponding $K(t)$ values according to Eq. (3) and the following Eq. (6):

$$K(t) = \frac{f C_1}{t^{1-f}},$$

(6)

where $K(t) = k(t)Q$, i.e., a corresponding product expressing the reaction rate in units of $s^{-1}$. $Q$ here is proportional to [B]. Figure 2 shows some examples of how $K(t)$ evolves with time, for different values of $f$. When $f = 1$, $K(t)$ is constant. When $f$ is small, $K(t)$ decreases fast at short times to reach an almost constant value at longer times. Because of this sort of variation of $K(t)$, we have chosen to give three of its representative values for each $f - C_1$ pair, i.e., its value $K_1$ (for channel #1), its value $K_\infty$ (for last channel), and its average value $\overline{K}$ over 200 channels. Thus the corresponding $K_1$, $K_\infty$, and $\overline{K}$ values are also given in Tables I and II. In case I, we notice that $f$ shows a small increase with $[B]_0/[A]_0$ ratio for $25 < s < 50$ but it stays practically invariant for the other two size ranges. On the other hand $C_1$, $K_1$, $K_\infty$, and $\overline{K}$ always increase with increasing $[B]_0$ in all size ranges examined. In case II, $f$, $K_1$, $K_\infty$, and $\overline{K}$ always increase with decreasing $[A]_0$.

Notice that all values of $f$ obtained are $< 0.66$, i.e., they never exceed the value 0.667 ($f = 0.667$ means that $d_s = 1.33$, which corresponds to the percolation threshold).[24] The values of $K_1$, $K_\infty$, and $\overline{K}$ are generally larger in case II than in case I. This goes along the total concentration of both A and B species, which is larger in case II than in case

TABLE I. Values of $f$, $C_1$, $K_1$, $K_\infty$, and $\overline{K}$ for various cluster sizes $s$ and various concentration ratios $[B]_0/[A]_0$ obtained by fitting Eq. (4) to the simulation data. Case I ($[A]$ = constant).

| $[B]_0/[A]_0$ | $f$ | $C_1$ | $K_1$ | $K_\infty$ $(10^6\ \mathrm{s}^{-1})$ | $\overline{K}$ |
|---|---|---|---|---|---|
| $25 < s < 50$ | | | | | |
| 1 | 0.59 | 0.017 | 9.9 | 1.2 | 1.9 |
| 2 | 0.61 | 0.031 | 18.8 | 2.4 | 3.8 |
| 5 | 0.62 | 0.075 | 46.3 | 6.3 | 9.8 |
| 10 | 0.65 | 0.092 | 66.7 | 8.8 | 14.0 |
| 20 | 0.65 | 0.115 | 74.7 | 11.7 | 17.7 |
| $25 < s < 250$ | | | | | |
| 1 | 0.64 | 0.006 | 3.6 | 0.5 | 0.8 |
| 2 | 0.62 | 0.012 | 7.4 | 1.0 | 1.5 |
| 5 | 0.64 | 0.026 | 16.8 | 2.5 | 3.9 |
| 10 | 0.63 | 0.054 | 34.4 | 4.9 | 7.6 |
| 20 | 0.66 | 0.119 | 78.3 | 12.8 | 19.1 |
| $25 < s < \infty$ | | | | | |
| 1 | 0.66 | 0.004 | 2.9 | 0.5 | 0.7 |
| 2 | 0.63 | 0.011 | 6.5 | 0.9 | 1.4 |
| 5 | 0.64 | 0.026 | 16.5 | 2.4 | 3.7 |
| 10 | 0.66 | 0.050 | 32.4 | 5.2 | 7.8 |
| 20 | 0.66 | 0.119 | 77.7 | 12.4 | 18.6 |



FIG. 2. Variation of $K(t)$ with time for various values of $f$.

I. In case II, no practical difference exists between the three different cluster-size ranges with respect to any of the calculated parameters, while in case I some differentiation is obtained for $25 < s < 50$.

The decay curves of $[A]$ vs time (similar to Fig. 1 of Ref. 22) are shown in Fig. 3 for different $[B]_0/[A]_0$ ratios together with the corresponding $f$ values. The data shown are for the range $25 < s < 50$ of case I.

TABLE II. Values of $f$, $C_1$, $K_1$, $K_\infty$, and $\overline{K}$ for various cluster sizes $s$ and various concentration ratios $[B]_0/[A]_0$ obtained by fitting Eq. (4) to the simulation data. Case II ($[B]_0$ = constant).

| $[B]_0/[A]_0$ | $f$ | $C_1$ | $K_1$ | $K_\infty$ $(10^6\ \mathrm{s}^{-1})$ | $\overline{K}$ |
|---|---|---|---|---|---|
| $25 < s < 50$ | | | | | |
| 1.0 | 0.50 | 0.134 | 67.3 | 4.8 | 9.1 |
| 1.5 | 0.55 | 0.131 | 72.4 | 6.4 | 11.3 |
| 2.0 | 0.58 | 0.125 | 71.9 | 7.6 | 12.7 |
| 4.0 | 0.61 | 0.123 | 74.8 | 9.4 | 15.0 |
| 10.0 | 0.64 | 0.118 | 75.0 | 10.9 | 16.8 |
| 20.0 | 0.65 | 0.117 | 75.7 | 11.7 | 17.7 |
| $25 < s < 250$ | | | | | |
| 1.0 | 0.51 | 0.135 | 68.9 | 5.1 | 9.6 |
| 1.5 | 0.56 | 0.131 | 72.7 | 6.9 | 11.9 |
| 2.0 | 0.58 | 0.127 | 73.7 | 8.0 | 13.3 |
| 4.0 | 0.63 | 0.120 | 75.1 | 10.4 | 16.0 |
| 10.0 | 0.66 | 0.114 | 75.2 | 12.4 | 18.5 |
| 20.0 | 0.66 | 0.119 | 78.3 | 12.8 | 19.0 |
| $25 < s < \infty$ | | | | | |
| 1.0 | 0.51 | 0.134 | 68.5 | 5.1 | 9.6 |
| 1.5 | 0.56 | 0.129 | 71.9 | 6.9 | 11.9 |
| 2.0 | 0.58 | 0.125 | 72.9 | 8.0 | 13.3 |
| 4.0 | 0.63 | 0.120 | 74.9 | 10.2 | 16.0 |
| 10.0 | 0.65 | 0.118 | 76.4 | 11.8 | 17.9 |
| 20.0 | 0.65 | 0.119 | 77.7 | 12.4 | 18.5 |

## B. Experimental data

The fluorescence spectra of pyrene embedded in DPPG small unilamellar vesicles (at lipid concentration $1-3.5 \times 10^{-4}$ M) were recorded at varying pyrene concentrations $[P]$. No excimer fluorescence could be recorded at $[P] < 10^{-6}$ M. The monomer decay time was then measured and found equal to 304 ns at 20 °C. Excimer fluorescence appeared progressively at $[P] > 10^{-6}$ M. At $[P] = 2 \times 10^{-5}$ M, the excimer to monomer fluorescence intensity ratio, $I_e/I_m$, (measured at 480 and 385 nm, respectively), reached 2.04, revealing an important excimer formation, whereas in a homogeneous solution (organic solvent) at this concentration, no excimer at all could be recorded. At a fixed pyrene concentration, the ratio $I_e/I_m$ increased where the lipid concentration decreased. We have assumed that pyrene was completely solubilized in the vesicle lipidic core, and, furthermore, that it did not practically affect the structure of the vesicles, at least in the sense that we treat here. The monomer fluorescence decay profiles (Fig. 1) have been recorded and fitted by the exclusive use of Eq. (5). The obtained results for some pyrene concentrations are given in Table III, for two lipid concentrations: $10^{-4}$ and $3.5 \times 10^{-4}$ M. Table III gives the values of the noninteger exponent $f$, of the average second-order rate $\bar{k}$, calculated according to Eq. (3), and of the average first-order rate $\overline{K}$, where $\overline{K} = \bar{k}[P]$. Notice that $f$ decreases when $[P]$ increases and the lipid concentration is $10^{-4}$ M but stays practically invariant when the lipid concentration is $3.5 \times 10^{-4}$ M. Interestingly enough, by assuming that 1 MSC (see Sec. III) is of the order of 1 ns, the simulated values of $\overline{K}$ are comparable with the experimental values (see Tables I–III).

The average second-order rate $\bar{k}$ decreased with increasing $[P]$ in both lipid concentrations examined. Notice that the experimental $f$ values are comparable with the calculated
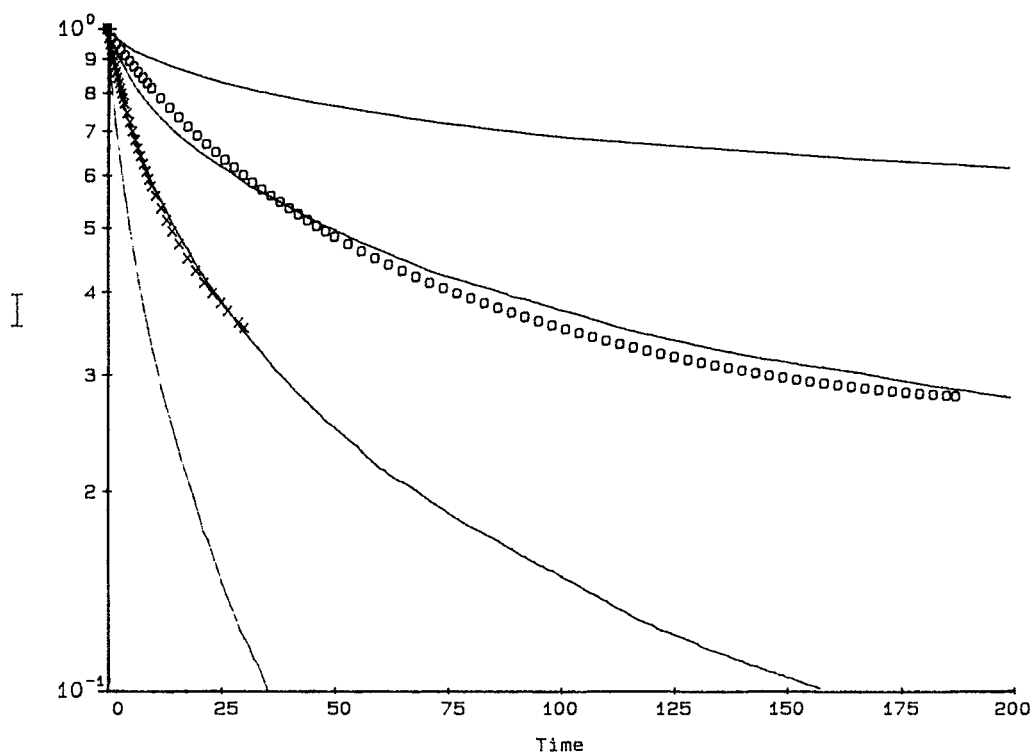
FIG. 3. Solid lines: plot of [A] vs MCS for $25 < s < 50$ of case I, for different $[B]_0/[A]_0$ ratios: (1) 2; (2) 5; (3) 10; and (4) 20. The corresponding $f$ values are: (1) 0.61; (2) 0.62; (3) 0.65; and (4) 0.65. $\square$ plot of the decay profile of $2 \times 10^{-5}$ M pyrene embedded in $3.5 \times 10^{-4}$ M DPPG deconvoluted from the contribution of the flash and corrected of the contribution of fluorescence. $\times$ same decay profile with the time scale contracted by a factor of 0.3.

values from the simulation data. For small lipid concentrations the $f$ values stay well below the percolation limit[24] of 0.67 (see above). For the higher lipid concentration the $f$ values stay close to the percolation limit, but below it. Finally, $K$ values are higher for the smaller lipid concentration. This is to be expected since higher first-order rates are naturally obtained when the ratio of the number of solubilizate molecules over the volume of the dispersed phase increases.

In Fig. 3 we plotted the experimental profile of $2 \times 10^{-5}$ M pyrene embedded in $3.5 \times 10^{-4}$ M DPPG together with the theoretical curves from the simulation calculations. The experimental profile has been first deconvoluted from the

contribution of the excitation pulse. Then it has been multiplied by $\exp(t/304)$, where $t$ is the time and 304 the decay time in ns, in order to eliminate the contribution of the fluorescence decay [cf. Eqs. (4) and (5)]. Figure 3 shows two curves of the same experimental profile, one as it is and the second at a time scale contracted by a factor of 0.3. This was done in order to stress the importance of the chosen time scale in comparing experimental data with simulation data which have arbitrary time units. Notice that the simulation data obtained with $[B]_0 = 5[A]_0$ of $25 < s < 50$ of case I (Table I) are very close to the experimental data. When the scale is contracted, the experimental data are very close to the data obtained with $[B]_0 = 10[A]_0$ ($25 < s < 50$, case I, Table I) up to ~30th MCS and very different at later times. This comparison shows that the simulation data can directly model the actual experimental system studied.

TABLE III. Values of $f$, $\bar{k}$, and $\bar{K}$ for various pyrene and lipid concentrations in SUV of DPPG at 20 °C (gel phase).

| Lipid concentration ($10^{-6}$ M) | Pyrene concentration ($10^{-6}$ M) | $f$ | $\bar{k}(10^{11}$ M$^{-1}$s$^{-1})$ | $\bar{K}(10^6$ s$^{-1})$ |
|---|---|---|---|---|
| 100 | 5 | 0.56 | 4.4 | 2.2 |
| | 10 | 0.45 | 3.9 | 3.9 |
| | 15 | 0.41 | 3.6 | 5.4 |
| | 20 | 0.35 | 3.5 | 6.9 |
| 350 | 5 | 0.65 | 2.5 | 1.3 |
| | 10 | 0.60 | 2.4 | 2.4 |
| | 15 | 0.61 | 1.8 | 2.7 |
| | 20 | 0.65 | 1.9 | 3.7 |
| | 30 | 0.62 | 1.4 | 4.3 |

## V. DISCUSSION

Both the experimental and the simulated data have allowed us with the use of Eqs. (3) and (4), to redefine and calculate the reaction rate in a geometrically restricted bimolecular reaction between a minority species A and a majority species B. This type of reaction is found, among others, in the fluorescence probing of organized assemblies. Here we focus on structures consisting of nonpercolating clusters and as such we have chosen the small unilamellar vesicles of DPPG at 20 °C, i.e., in its gel phase. We now discuss the obtained results and make comparisons between the simulated and experimental ones.

Case I of simulation corresponds to an experimental situation where a minority species A is solubilized in the interior of isolated clusters together with the species B. We treat several cases, where $[A]_0$ remains constant while $[B]_0$ progressively increases. The increasing presence of B particles makes reaction between A and B particles easier, therefore the values of the reaction rate expressed in first order, i.e., $K(t)$ (given by $K_1$, $K_\infty$, and $\overline{K}$ in Table I) increased progressively by almost an order of magnitude. The same situation arises with pyrene in vesicles, where [A] corresponds to excited and [B] to unexcited pyrene. The progressive increase of $\overline{K}$ for pyrene is not so extensive as for the reaction between A and B, apparently, because the concentration [P] was not high enough. Further increase of [P] is limited by solubility and also by monomer pyrene self-absorption.

The simulation results for the exponent $f$ do not predict any variation of $f$ with increasing [P] or, in the limit, they predict some small increase. It is then interesting to record an unexpected decrease of $f$ with increasing [P] at low vesicle concentration. This result leads us to the following conclusion: At small lipid (and vesicle) concentration, the number of pyrene molecules solubilized in the same vesicle is relatively high. Then it is possible to obtain an excited pyrene molecule in the close vicinity of an unexcited one, and the excimer formation to be facilitated so to appear as static. The "dynamic" aspect of such a quasistatic interaction is a fast decrease of fluorescence intensity leading to a steeper decrease of the decay profile. In such cases $f$ values appear smaller. Of course, this phenomenon is favored at higher pyrene concentrations, explaining the trends obtained in Table III for $10^{-4}$ M DPPG.

The results of case II of simulation come in verification of the above conclusions. In Table II, smaller $f$ values are obtained when the reaction domain is highly populated by the reacting species, i.e., when $[B]_0/[A]_0 = 1.0$ ($[A]_0 = [B]_0 = 2000$ particles), and this fact is not related with the cluster size, i.e., it is true for all cluster-size ranges. In other words, when the reaction domain is highly populated by the reacting species the obtained values of $f$ do not reflect the geometry of the reaction domain itself but rather the geometry of the (forced) particular distribution of the solubilizates. For this reason, case II is not a "well-behaving" system, therefore the $K$ values vary in rather unexpected trends, i.e., increase with decreasing concentration $[A]_0$. At any rate, Fig. 2 shows that higher $K$ values are obtained with higher $f$ values. Nevertheless, $K$ was high at $[P] = 2 \times 10^{-5}$ M, even though $f$ was low. Obviously, in this real experimental system, the increase of the rates due to increasing presence of quenchers prevails (cf. comments on the variation of $k$ given below).

The choice of the density $p = 0.50$ of free sites for the simulation model was made in order to obtain $f$ values close to the experimental ones. The fact that these values are close to the percolation limit tempts us to conclude that with $3.5 \times 10^{-4}$ M of DPPG one obtains a vesicle-dispersed phase which is not far from the corresponding percolation limit. Thus, with smaller lipid concentration, $f$ values go away from the percolation limit even at small pyrene concentrations.

The decrease of the second-order reaction rate $\overline{k}$ with increasing [P] in Table III is a particularity of the restricted reaction spaces. Increase of [P] means decrease of the available free sites per quencher. Thus, even though the quenching species becomes more abundant facilitating first-order kinetics, the probability for a single quencher to reach the fluorophore decreases, making second-order kinetics slower.

Finally, the direct comparison of the simulation and the experimental data of Fig. 3 shows that the real experimental situation can be well approximated by computer simulation. Notice that the experimental value of $f$ for $2 \times 10^{-5}$ M pyrene in $3.5 \times 10^{-4}$ M DPPG is 0.65. Furthermore, the data of Table III for $3.5 \times 10^{-4}$ M DPPG show that any value above 0.60 is permissible for the decay of pyrene, within experimental error. Notice also that for the close lying curve (2) of Fig. 3, $f = 0.62$, i.e., the experimental and the simulated $f$ values are practically equal. The $\overline{K}$ value that corresponds to the same simulated curve is $9.8 \times 10^6$ s$^{-1}$ (Table I) while for the experimental curve $\overline{K} = 3.7 \times 10^6$ s$^{-1}$ (Table III). The two values are of the same order of magnitude. Their difference is just a question of time scale.

## VI. CONCLUSIONS

We have studied the bimolecular reaction between a majority species B and a minority species A both by simulation and by fluorescence probing of small unilamellar vesicles with pyrene. Thus, a picture is introduced that models these systems as nonpercolating structures, where reactions proceed within an isolated cluster (vesicle) without exchange between clusters.

The analysis of the data was done with the use of Eqs. (4) and (5) and has helped us to redefine the reaction rate in restricted geometries through Eqs. (3) or (6). Our focus in the present work is the behavior of the time-dependent rate constant of the reaction for various initial conditions (concentrations). The clusters may or may not be fractal objects. In any case the analysis depends on the calculation of the spectral dimension of the random walk of the reacting species. The reaction rate is time dependent, and it depends also on the spectral dimension. Both the equivalent first-order and second-order rates can be taken into account.

The experimental situation of excited pyrene in the presence of unexcited pyrene in SUV can be represented by case I of simulation where the reactant concentration is sufficiently low. At small lipid concentration, a quencher-concentration effect is detected. However, when lipid concentration is high enough, there exists no concentration effect. At any rate, the first-order rate $K(t)$ was larger when [P] is larger in all cases examined.

The values of $f$ stayed below the theoretical limit for percolation, but they approached it when lipid concentration was high. The exclusive use of Eq. (4) to fit data is true for both the simulation and for the present experimental data as well as with all other data with pyrene in vesicles studied so far.

## ACKNOWLEDGMENTS

[1] D. Pines and D. Huppert, Chem. Phys. Lett. **156**, 223 (1989).

[2] J. M. Drake and J. Klafter, Phys. Today **43**, 46 (1990).

[3] D. Pines, D. Huppert, and D. Avnir, J. Chem. Phys. **89**, 1177 (1988).

[4] P. Levitz, J. M. Drake, and J. Klafter, J. Chem. Phys. **89**, 5224 (1988).

[5] S. Havlin and D. ben-Avraham, Adv. Phys. **36**, 695 (1987).

[6] A. Blumen, J. Klafter, and G. Zumofen, Phys. Rev. B **28**, 6112 (1983).

[7] J. Klafter and A. Blumen, J. Chem. Phys. **80**, 875 (1984).

[8] R. Kopelman, J. Stat. Phys. **42**, 185 (1986).

[9] P. Argyrakis and R. Kopelman, J. Chem. Phys. **84**, 1047 (1986).

[10] A. Blumen, G. Zumofen, and J. Klafter, in *Fractals, Quasicrystals, Chaos, Knots, and Algebraic Quantum Mechanics*, edited by A. Amann, L. Cederbaum, and W. Gans (Kluwer Academy, Dordrecht, 1988), p. 21.

[11] A. Blumen, J. Klafter, and G. Zumofen, in *Optical Spectroscopy of Glasses*, edited by I. Zschokke (Reidel, Dordrecht, 1986), p. 199.

[12] L. W. Anacker, R. P. Parson, and R. Kopelman, J. Phys. Chem. **89**, 4758 (1985).

[13] P. Lianos, J. Chem. Phys. **89**, 5237 (1988).

[14] G. Duportail and P. Lianos, Chem. Phys. Lett. **149**, 73 (1988).

[15] G. Duportail and P. Lianos, Chem. Phys. Lett. **165**, 35 (1990).

[16] P. Lianos and G. Duportail, Appl. Fluoresc. Technol. **2**, 15 (1990).

[17] P. Lianos and S. Modes, J. Phys. Chem. **91**, 6088 (1987).

[18] P. Lianos, Prog. Coll. Polym. Sci. **76**, 140 (1988).

[19] S. Modes, P. Lianos, and A. Xenakis, J. Phys. Chem. **94**, 3363 (1990).

[20] P. Lianos and A. Malliaris, Israel J. Chem. (in press).

[21] G. Zumofen and A. Blumen, Chem. Phys. Lett. **88**, 63 (1982).

[22] P. Lianos and P. Argyrakis, Phys. Rev. A **39**, 4170 (1989).

[23] P. Argyrakis and R. Kopelman, J. Phys. A **21**, 2753 (1988).

[24] S. Alexander and R. Orbach, J. Phys. (Paris) **43**, L625 (1982).